THE JOURNAL OF PHYSICAL CHEMISTRY C
A JOURNAL OF THE AMERICAN CHEMICAL SOCIETY

pubs.acs.org/JPCC

Article

Increased Sensitivity and Selectivity for As(III) Detection at the Au(111) Surface: Single Crystals and Ultraflat Thin Films Comparison

Published as part of The Journal of Physical Chemistry virtual special issue "Esther Sans Takeuchi Festschrift".

Tybur Q. Casuse-Driovínto,* Rubén Rizo, Angelica Benavidez, Adrian J. Brearley, José M. Cerrato, Fernando H. Garzon,* Enrique Herrero, and Juan M. Feliu

Cite This: https://doi.org/10.1021/acs.jpcc.2c05541

Read Online

ACCESS | Metrics & More | Article Recommendations | Supporting Information

ABSTRACT: Electrochemical stripping voltammetry electroanalysis sensitivity and selectivity are oftentimes limited by wide variance in analyte electrode surface adsorption and desorption energies. The use of highly oriented Au(111) single crystal and thin film surfaces is shown to decrease this variance and improve detection for arsenic (As) in water. Cyclic voltammetry and linear stripping voltammetry (LSV) analysis on Au oriented and polyoriented electrode surfaces demonstrated that As deposition and oxidation is a complex surface-structure-dependent process. An electrochemical quartz microbalance indicated that As is deposited in multiple layers when in high concentrations and does not permanently reorganize the Au surface after stripping. LSV analysis of As(III) on the Au(111), Au(110), Au(100), and Au polyoriented single crystal, Au(Poly), model electrode surfaces showed that Au(111) had the highest peak to background ratio and narrowest peak width for As oxidative stripping. Furthermore, an ultraflat Au(111) thin film, Au(UTF), was then compared to the Au(111) and Au(Poly) single crystals and showed a bulk Au(111) single crystal-like response. The Au(UTF) was then used to perform a calibration curve to detect between 2.5 and 100 $\mu g\ L^{-1}$ As(III) and resulted in a theoretical limit of detection of 0.0065 $\mu g\ L^{-1}$ in 0.5 M H_2SO_4. The results from this study indicate that the Au(UTF) surface provides the sensitivity necessary for detection of trace concentrations of As in water at or below the maximum contaminant level (MCL) of 10 $\mu g\ L^{-1}$.

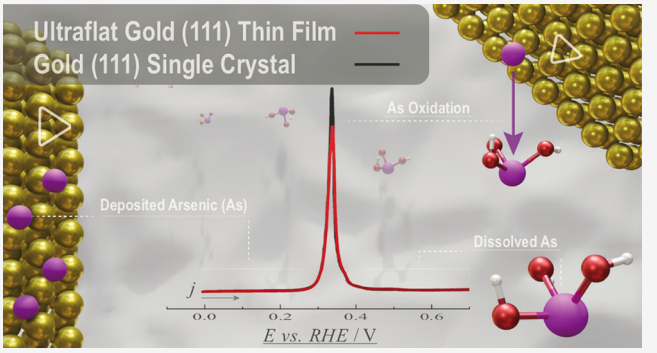

INTRODUCTION

The ability to detect arsenic (As) at parts per billion (ppb) concentrations is essential to informing populations around the world with potential exposures to As contamination about the safety of their drinking water.[1−3] The maximum contaminant level (MCL) set by the World Health Organization and the United States Environmental Protection Agency for safe daily drinking water is 10 ppb, or $\mu g\ L^{-1}$.[4,5] Concentrations above this can lead to cancer in numerous organs, as well as adverse cardiovascular or neurological effects. Arsenite, As(III), is expected to be in the form of H_3AsO_3 in reducing and acidic conditions.[6] Arsenite is considered to be the most toxic aqueous form of As in comparison to arsenate, As (V), and other methylated forms.[7] Although oxyanions of As(V) are considered to be electro-inactive, the concentration of As(V) has been electrochemically determined by measuring the difference in concentration of As(III) before and after chemical reduction methods.[8] The growing overabundance of As in drinking water sources due to natural and anthropogenic mobilization calls for development of broadly available, portable, and highly sensitive and selective As sensing systems.[9−13]

Electrochemical detection of trace concentrations of As in water has been investigated using gold (Au) electrodes with a broad variety of morphologies and generation methods seeking to improve detection capabilities.[13−16] Electrochemical sensing has several benefits over common laboratory methods, such as inductively coupled plasma (ICP) mass spectrometry, ICP atomic emission spectroscopy, and atomic absorption spectroscopy, including the ability to provide in situ quantitative analysis, decreased cost, and portability.[17−22] Sensing electrodes have been generated using electrodeposition, chemical nanoparticle deposition, and physical vapor deposition to form macro- and nanoscale structures capable of detecting well

Received: August 3, 2022
Revised: October 23, 2022

below the MCL in water.[14,23−31] Identifying new electrode materials and understanding factors affecting sensitivity and selectivity for As detection have been the focus of a growing body of research since pioneering works produced by the Compton group and others over the past few decades.[14,24,32−38] Han et al., Ren et al., and others have sought to understand the effects of surface orientation on the electrochemical detection of heavy metals. Surfaces with controlled crystallographic surface orientation have been generated by several methods including shaped nanoparticles, dendrites, selective blocking, the Clavilier method, and the Czochralski method.[32,39−44] Significant advances in texture-oriented electrode generation and availability have been made; however, the development of ultraflat, thin film Au(111) electrodes for electroanalysis has received relatively little attention.[45−47] The use of Au as an electrode material for electroanalysis is ubiquitous with a vast number of publications and variety of applications available. However, to the best of our knowledge, the utilization of ultraflat (111) thin films for electroanalysis has not been extensively explored. Existing research utilizing ultraflat Au(111) thin films has focused primarily on use as a substrate for nanoscale fabrication of other materials,[48−50] and there has not been a single study developing ultraflat Au(111) thin films for aqueous metals detection.

Single crystal electrochemical studies provide valuable insights into reaction mechanisms including electron transfer,[51,52] adlayer adsorption and desorption,[53−58] and catalytic activity for a wide variety of adsorbates which are impacted by site geometry.[33,59] The use of Au nanoparticles and nanostructured electrodes benefit from decreased precious metal consumption per electrode and have been shown to provide high sensitivity for As(III) detection. The use of nanoparticles with a three-dimensional structure inevitably includes imperfections in crystallographic orientation due to the edges of the nanoparticles and variation in size and shape during the synthesis processes. Single crystal surfaces with minimal imperfections provide clearer insight into structure−activity−selectivity relationships which directly benefits electroanalytical studies seeking to identify materials with high sensitivity and selectivity.[56,60] At the time of this article there has not been an investigation comparing As(III) deposition and stripping on Au(111), Au(110), Au(100), and polyoriented single crystal surfaces.

Limited commercial accessibility and utilization of high sensitivity and selectivity electrochemical As(III) sensors is perplexing considering the substantial amount of literature produced over the past few decades on the subject.[21,61,62] Many studies develop complex, innovative, and unique methods to generate novel electrodes for As(III) detection with excellent limits of detection.[63,64] However, there is growing interest in considering the applicability of these methods to address the global need for localized arsenic detection in water.[20,65−69] It is essential that the availability of in situ arsenic sensors be addressed by identifying manufacturable, automatable, and accessible electrodes and sensing systems so our scientific community can bring this highly capable and viable public health resource to the people who need it most.

The objective of this study is to develop understanding of commercially available ultraflat Au(111) thin films, Au(UTF), and the capability to provide single crystal-like detection for trace As(III) in water by identifying the impact of surface structure on As(III) redox at well-oriented Au surfaces. In this study we provide insight into the redox behavior of As(III) at single crystal surfaces with cyclic voltammetry (CV) and linear stripping voltammetry (LSV) analysis. A quartz crystal microbalance (QCM) was used to perform CV studies with a Au(111)-oriented film to provide further insight into As(III) adlayer formation. The Au(UTF) was characterized using microscopy, diffraction techniques and electrochemical comparison to the model electrodes and then utilized to detect trace concentrations of As(III) in 0.5 M sulfuric acid solutions. This study provides new insights into the influence of surface structure on the selectivity and sensitivity for As(III) electrochemical detection at Au surfaces to develop well-oriented Au thin films as a reproducible and commercially available electrode which can provide single crystal-like detection capabilities using ultralow Au loadings per electrode. This study is the first to report that ultraflat Au(111)-oriented thin film electrodes duplicate or exceed the behavior of Au(111) crystal surfaces for high sensitivity and selectivity electroanalysis of As(III) in water. The results of this study advance aqueous electroanalysis capabilities for LSV detection of As, and potentially other redox active metal(loid)s, which can impact large scale development of sensor technologies.

EXPERIMENTAL SECTION

Materials Description and Characterization. *Physical Characterization. Single Crystals.* Clavilier's method was used to generate basal plane Au single crystal model surface electrodes for the Au(111), Au(110), and Au(100) orientations.[56,70] A 0.5 mm Au wire was held vertically and melted using a controlled torch to form a bead at the end of the wire which was then slowly cooled to form a single crystal. The single crystal bead was then mounted in a four-cycle goniometer and oriented using the laser reflections from the surface facets. Then the Au bead was coated in epoxy for stabilization, cut with emery paper to a flat surface, which had the selected orientation, and polished with diamond paste until a mirror finish was obtained. The polyoriented Au single crystal, hereafter referred to as Au(Poly), was an uncut single crystal bead and represents the multiple orientations present in a single crystal.

Ultraflat Au(111) Thin Film. The Au(UTF) films (Platypus Technologies) were physically characterized using S/TEM, electron backscatter diffraction (EBSD), pole figures, atomic force microscopy (AFM), and XRD (Figure S1A−F, Figure S2) and showed a strong Au(111) preferred orientation. Electron backscatter diffraction images were collected using a FEI Helios 600 NanoLab FEGSEM-FIB at the Nanoscale Characterization and Fabrication Laboratory (NCFL) at Virginia Tech. A JEOL NEOARM 200 kV aberration-corrected scanning transmission electron microscope (S/TEM) at UNM was used for film grain structure visualization (Figure S1A). The films were highly (111) textured, polycrystalline materials with grains rotationally disordered parallel to the substrate surface. Platypus Technologies quotes a film thickness near 100 nm and an average grain area of 3.64 ± 0.2 μm^2.[47] During EBSD analysis, charging image distortion effects can be observed in Figures S1B. Figure S1B presents the EBSD data showing that the grains are predominantly oriented in the Au(111) direction as shown by the legend in Figure S1E. The [100] pole figure shows a circle of points in Figure S1C which indicates that the grains in the thin film are randomly oriented in their in-plane directions. The inverse pole Figure S1D shows

https://doi.org/10.1021/acs.jpcc.2c05541
J. Phys. Chem. C XXXX, XXX, XXX−XXX

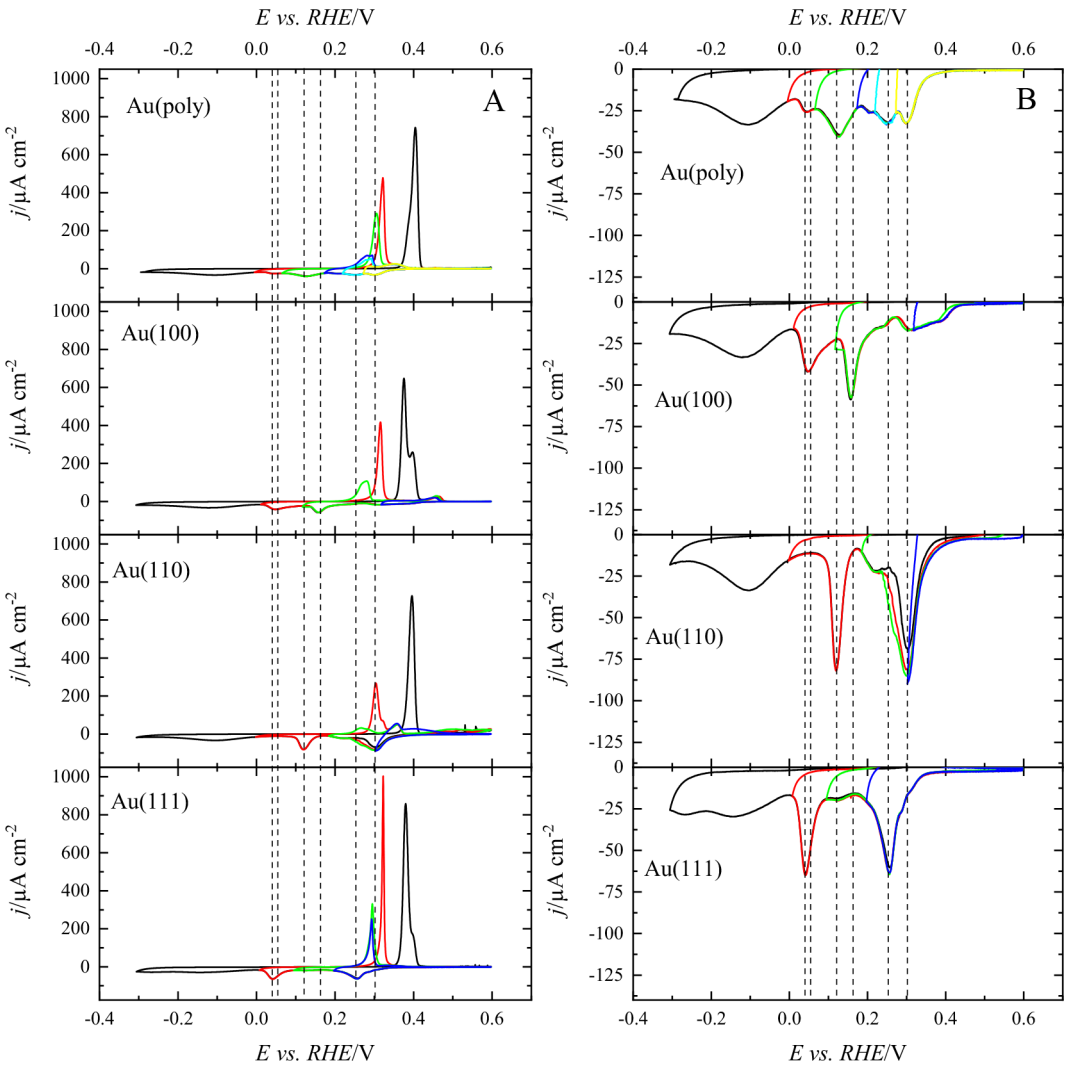

Figure 1. Cyclic voltammograms for the different Au electrodes in 0.5 M H_2SO_4 + 1 mM As(III) with different lower limits. Scan rate: 10 mV s^{-1}. The vertical lines mark the position of different deposition peaks on the electrodes. (A) Full cyclic voltammogram. (B) Enlarged graph to show the detail of the As(III) deposition process.

that the vast majority of the domains are oriented in the Au(111) direction. Surface roughness was characterized by atomic force microscopy (AFM) using a WiTec Alpha300R. The AFM image of the Au(UTF) surface shows that the surface is very flat with variations in a 30 nm range across the image (Figure S1F). The root-mean-square (RMS) roughness is quoted by the manufacturer as 0.36 nm; however, our analysis found it to be 2.6 nm using Gwyddion measurements (Table S1).

Quartz Crystal Microbalance Electrode. Quartz crystal resonator QA-CL3 dip cells and a QCM943 oscillation circuit unit were obtained from Princeton Applied Research to collect electrochemical quartz crystal microbalance (EQCM) measurements. The surface normal orientation was determined using thin film Bragg diffraction (PanAnalytical X'Pert Pro) equipped with a multilayer X-ray mirror. The Au film on the EQCM showed strong (111) normal orientation (Figure S2).

Electrochemical Characterization. Electrochemical experiments were carried out in a two-compartment electrochemical glass cell, using a Au wire as a counter electrode and a reversible hydrogen electrode (RHE) as a reference electrode. Voltammetric experiments were carried out at room temperature using a wave signal generator (EG&G PARC 175), potentiostat (eDAQ 161), and digital recorder (eDAQ e-corder 401) workstation. All solutions were made using ultrapure water (18.2 MΩ cm, Elga PureLab Ultra), concentrated sulfuric acid (VWR, 95 wt %), and As_2O_3 salt (Merck). A stock solution of 10^{-1} M As(III) in 0.5 M H_2SO_4 was used to prepare lower concentration solutions.

Single Crystals. The basal plane single crystals were connected to the solution using the hanging meniscus method so that the polished flat part of the single crystal bead was the only surface touching the solution. The Au(Poly) electrode was submerged into the solution so that the wire was minimally interacting with the solution. The electrochemical surface areas of the Au(Poly), QCM, and Au(UTF) electrodes were determined using the charge of the Au reduction peak from cyclic voltammetry at 10 mV s^{-1} up to 1.7 V. The reference value used was 660 μC cm^{-2}, which represents a three-electron transfer process per Au(111) surface atom with a specific current of 220 μC cm^{-2} per electron transferred. The surface area of the single crystal basal plane surfaces was determined using optical microscopy of the flat area prior to use. Prior to any electrochemical experiment, the electrode was

https://doi.org/10.1021/acs.jpcc.2c05541
J. Phys. Chem. C XXXX, XXX, XXX−XXX

annealed in a propane/oxygen flame and quenched using ultrapure water to remove any organics that may have been adsorbed on the surface and to restore the surface order. A protecting droplet of ultrapure water was left on the single crystal surface when the electrode was transported into the cell. After performing analysis in As-containing solutions, the electrode was quenched and annealed using concentrated nitric acid to ensure all As was chemically stripped off the electrode surface.

Ultraflat Au(111) Thin Film. The Au(UTF) electrodes were compared to single crystal model electrodes for their Au redox behavior using cyclic voltammetry (Figure S1G). The Au(UTF) electrode was removed from the substrate according to Platypus Technologies instructions directly prior to use and partially submerged in a solution of 0.5 M H_2SO_4. Figure S1G presents a comparison of the characteristic Au redox peaks for the Au(UTF) and the basal plane surfaces which are similar to expected peaks from previous research.[71] The Au redox profiles of Au(UTF) and Au(111) both begin with a shoulder in the positive sweep direction beginning at 1.4 V which leads to a peak at 1.6 V for Au oxidation, showing that the Au(UTF) has a Au(111) single crystal-like electrochemical response.

Quartz Crystal Microbalance Electrode. The QA-CL3 dip cell was used to perform cyclic voltammetry studies of As reduction and oxidation. The Sauerbrey equation (eq 1) was used to convert between the frequency and mass.

$$\Delta F = -\frac{2f_0^2}{A\sqrt{\rho_q \mu_q}}\Delta m \quad (1)$$

where ΔF is the change in frequency, f_0 is the standard frequency of 9 MHz, A is the area of the electrode surface, 0.174 cm^2, ρ_q is the density of the quartz crystal, μ_q is the shear modulus of the quartz crystal, 2.947×10^{11} g cm^{-1} s^{-2}, and Δm is the change in mass.

Statistical analysis was performed in EXCEL to determine average and standard deviation of three consecutive measurements where applicable. Linear stripping voltammetry was smoothed using a Lowess method with a span of 0.01 for clarity in the image. The raw data were used to calculate the calibration plot of concentration vs charge density. Limits of detection were determined using the equation LOD = $(k \times Sb)/m$, where k is equal to 3 for a 98.3% confidence level, Sb is the standard deviation for analysis of three blank curves, and m is the slope of the calibration curve.

RESULTS AND DISCUSSION

Arsenite Deposition/Dissolution on Au Electrodes. Figure 1 shows the voltammetric profile of a polyoriented Au electrode immersed in a 10^{-3} M As(III) solution. As can be seen, in the deposition process up to −0.3 V vs RHE (potential at which hydrogen evolution starts) several peaks can be detected in the negative scan direction which have been reported in previous studies as well.[72] The presence of several deposition peaks suggests the presence of a complex deposition process, in which the presence of a bare Au surface or a previous As adlayer alters the dynamics of the process. It should be noted that this voltammogram is stable upon cycling between these potential limits. Also, the deposition currents are significantly smaller than those expected for a diffusion-controlled process. In fact, currents recorded in 0.1 M As(III) solutions are similar to those recorded here (Figure S3 and Table S2), implying that the deposition is controlled by the kinetics of the process, explaining the presence of several deposition peaks. On the other hand, a main single peak is observed in the dissolution process of As. Because the deposition process is determined by the kinetics, the structure of the adlayers formed can have a significant impact on the dissolution process. To establish such an effect, voltammograms with different potential limits between 0.2 and −0.3 V were recorded (Figure 1 and S4). As the lower potential limit is made more negative, the As stripping peak shifts progressively to higher potential values, which indicates that the dissolution of the As layer is governed by the topmost layer. Dinan et al. found that deposition below 0 V vs RHE is likely controlled by a high field growth mechanism and that, above two or three monolayers, As begins to build a passivating amorphous layer.[72] The study also observed that the stripping peak was a function of the lower potential limit and ramp rate; however, the reasoning for this was not explained. The high field growth mechanism is highly dependent on the binding energy of adsorbing atoms to the structure of the layer beneath.[73,74] Because plating potential is the only factor impacting the positive shift in the stripping peak and it is occurring most prevalently below 0 V vs RHE, the binding energy of subsequent As atoms to the layer beneath must be increasing. A restructuring of the surface to a more densely packed and stable layer when electrochemically adsorbing As after epitaxially oriented monolayers may be the cause, but further studies would need to confirm this.[75,76]

This type of deposition/dissolution process, which is dependent on the nature of the layer underneath, is expected to depend also on the surface structure of the electrode. For this reason, As(III) deposition/dissolution was studied on Au single crystal electrodes (Figure 1). Although the qualitative behavior is the same as that observed for the Au-polyoriented electrode, significant differences can be observed between the different surfaces. This fact clearly indicates that the deposition process is a surface-sensitive process. At potentials higher than 0 V on the single crystal electrodes, two main peaks are observed for the deposition process, followed by a wider peak below this potential. Tentatively, the first two peaks can be assigned to the formation of the two first layers of As, and the peak at $E < 0$ V represents the formation of a massive As film. As shown in Figure 1B, which is an enlargement of the deposition scan of Figure 1A, each of the peaks observed in the Au(111), Au(100), and Au(110) electrodes has its corresponding peak on the polyoriented electrode (in some cases, two of the peaks corresponding to the single crystal electrodes overlap in the polyoriented surfaces). Thus, it can be considered that the voltammogram of the polyoriented electrode is the result of the contributions of the different facets and ordered domains. In contrast, only one peak is observed in the dissolution. As happens in the polyoriented surface, the potential of the dissolution peak depends on the lower potential limit and the extension of the As deposition.

It should be noted that the standard potential of H_3AsO_3 reduction to As(0) is 0.248 V vs SHE, which means that the equilibrium potential of this redox couple in this medium is ca. 0.24 V. This fact implies that any deposition process taking place at higher potentials is an underpotential deposition (UPD) process.[77,78] As can be observed in Figure 1B, the onset for As deposition is higher than this value for all the surfaces. However, clear peaks related to the As UPD deposition are only observed for Au(110) and Au(100) single crystal electrodes. Underpotential deposition of As(III) onto Au

https://doi.org/10.1021/acs.jpcc.2c05541
J. Phys. Chem. C XXXX, XXX, XXX−XXX

electrodes has been observed and utilized by other researchers for electrochemical As detection and formation of gallium arsenic (GaAs) layers.[33,79] Figure S4 shows an enlargement of this region for cycles with lower limits larger than 0 V. Clearly, dissolution peaks at 0.36 and 0.45 V for the Au(110) and Au(100) electrodes, respectively, are observed, which corresponds to the dissolution of the UPD processes and confirms previous study findings.[79] For the Au(111) electrode, although the deposition starts at a higher potential, there is no well-defined deposition peak below this potential and the main peak potential is ca. 0.25 V, which suggests that it contains contributions only from the normal deposition process. For the Au(Poly) electrode, the UPD dissolution process is observed due to the presence of (100) and (110) domains in the polyoriented surface.

Charge curves for the deposition process are shown in Figure 2. As can be seen, total charges at −0.3 V (the lower limit for the deposition process) are very similar for all the electrodes, standing for ca. 1700 μC cm^{-2}. For the Au(111) surface, the measured charge at 0.1 V, just after the first deposition peak, stands for ca. 624 μC cm^{-2}. Taking into account that a process transferring one electron per Au(111) surface atom exchanges 220 μC cm^{-2}, and three electrons are exchanged in the As(III) deposition process, it can be proposed that, after the first deposition peak, a pseudomorphic (1 × 1) As layer has been formed. Villegas et al. also observed (1 × 1) adsorption on Au(111) crystal surfaces using Auger electron spectroscopy.[79] After the second deposition peak centered at 0.045 V, the deposition charge at 0 V is ca. 1000 μC cm^{-2}, which suggests that this second peak is related to the formation of the second layer. From that point, multilayer deposition would occur in the third and broad peak. For the Au(100) and Au(110) surfaces, the situation is similar to that observed for the Au(111) electrode, and thus each peak should correspond to the deposition of the first and second layers. It should be noted that the final charge is very similar for all the electrodes, although at intermediate potentials they differ. This implies that, during the deposition of the third and subsequent layers, the underlying Au structure does not affect the deposition process and only the deposition of the first two layers depends on the Au structure.

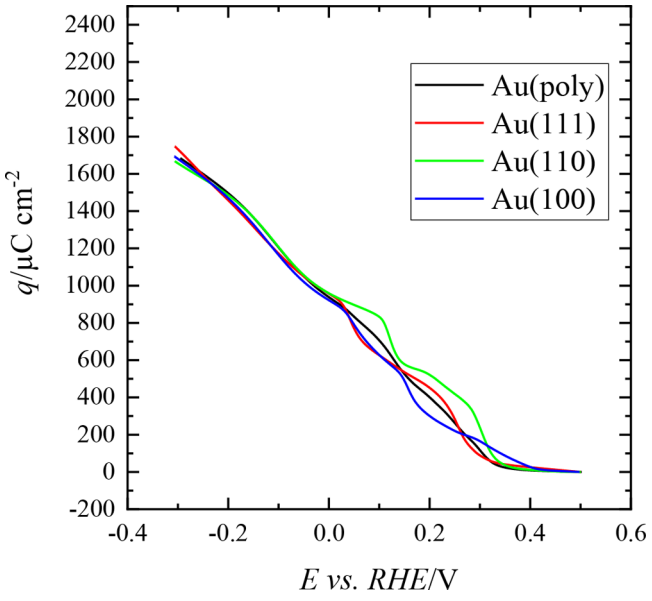

Figure 2. Integrated charges measured during the deposition scan for the different Au electrodes using the voltammetric curves in Figure 1.

Electrochemical QCM experiments were carried out to determine the nature of the deposited adlayer. Figure 3 presents the evolution of the QCM frequency and current density during the cyclic voltammetry of a Au film electrode in 10^{-3} M As(III). The QCM surface showed a highly Au(111)-preferred surface orientation in XRD analysis (Figure S2), and the Au redox prior to introduction of As to the solution also showed a degree of preferred Au(111) orientation due to the primary Au oxidation peak being at 1.6 V (Figure S5).[71] As shown in Figure 4A, the frequency returns at the initial value after one complete cycle, indicating that the only process occurring is related to the As deposition/dissolution. The mass of the deposition species can therefore be determined from the ratio between the frequency change and the charge. Figure 4B presents the comparison between the deposition current, the integrated charge density, and the mass adsorbed onto the Au surface. The mass changes and the integrated charge curves overlap, which implies that the stoichiometry of the deposition process is the same in the whole potential window. Additionally, the ratio between the deposition change and mass between 0.2 V and −0.3 V is about 15 g (mol e$^-$)$^{-1}$. In the reduction process of As, three electrons are exchanged,

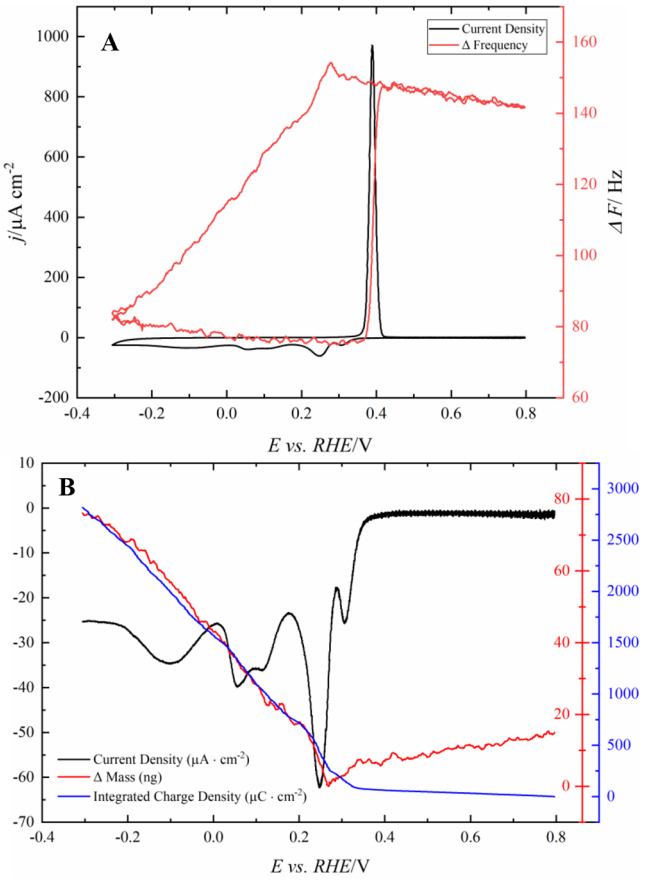

Figure 3. Electrochemical quartz microbalance during cyclic voltammetry in 0.5 M H_2SO_4 + 1 mM As(III) with supporting electrolyte. (A) Current density and change in crystal frequency vs potential during CV at 10 mV s^{-1}. (B) Current density, charge density, and change in mass vs potential during deposition of As(III) at the QCM surface.

https://doi.org/10.1021/acs.jpcc.2c05541
J. Phys. Chem. C XXXX, XXX, XXX−XXX

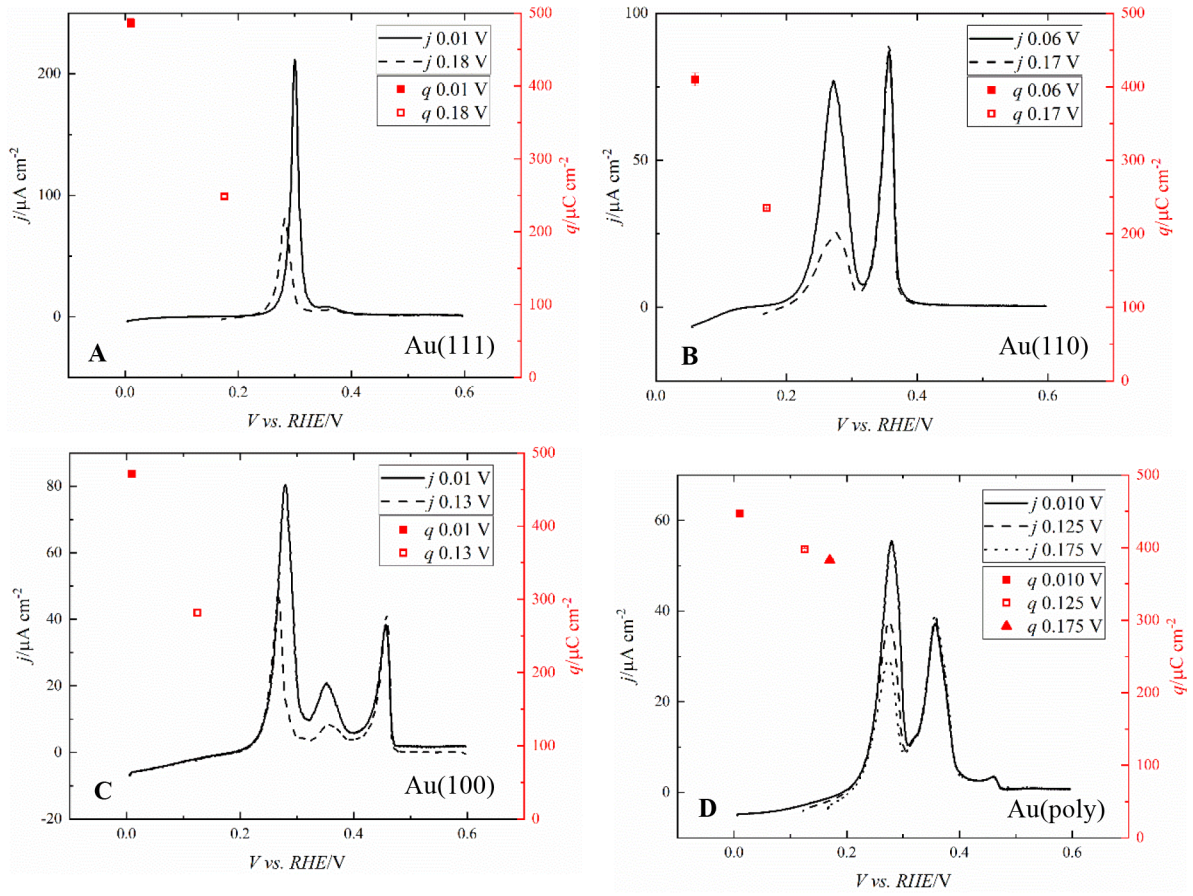

Figure 4. Arsenic stripping voltammograms for the different electrodes: (A) Au(111); (B) Au(110); (C) Au(100); and (D) Au(poly), in 0.5 M H_2SO_4 + 10^{-5} M As(III). The electrode potential was held for 60 s at the depositing potentials shown in the legends. The scan rate is 10 mV s^{-1}. The red dots in the figure represent the integrated charge (right-hand axis).

which implies that the molar mass of the depositing species is 45 g mol^{-1}. This value is lower than the atomic mass of As (75 g mol^{-1}), which suggests that in the deposition-process-adsorbed water molecules have been displaced from the interface. Considering the difference between the measured molar mass and the As molar mass (75−45 = 30 g mol^{-1}), approximately two water molecules have been displaced from the interface per As atom deposited. Huang et al. also observed a weakly bound adsorbate which was stripped off of the Au surface during EQCM studies.[80]

Now that the electrochemical behavior of As on Au electrodes has been established, the possible use of these electrodes for chemical analysis of As(III) in solution can be tested. For that purpose, the different electrodes were held at different potentials for 60 s and the stripping curve was recorded for 10^{-5} M As(III) in 0.5 M H_2SO_4 (Figure 4). Two potentials were chosen for the basal planes, each one after the first two deposition peaks, and three potentials were evaluated for the polyoriented Au electrode. Important differences have been observed between the profiles of the four electrodes. While the Au(111) electrode showed a single sharp peak the Au(110), Au(100), and polyoriented electrodes showed more complex oxidation processes. Table 1 summarizes the main data for the experiment. For Au(100), three peaks are observed whereas for Au(110), two peaks can be distinguished. In fact, the observed behavior for the stripping peaks is very similar to that obtained for the positive scan direction of the voltammetric experiments in 10^{-3} M As(III) solution using a similar lower limit for the scan (Figures 1 and S4). The only notable difference is the small shift in the peak potentials due to the difference in concentration of the solution. Using this information, we can assign the peaks at 0.450 V for the Au(100) electrode and at 0.360 V for the Au(110) electrode to the dissolution of the UPD layer,[81] because these peaks are still visible when the lower limit of the scan is above 0.3 V, that is, when bulk As deposition is still not thermodynamically favorable. Thus, the observed difference between the Au(111) electrode and the rest of the surfaces is that no UPD phenomenon is observed on the Au(111). In the case of the polyoriented Au electrode, the observed behavior is the weighted combination of the electrochemical behavior of the different sites present on the surface. Many studies using polyoriented electrodes present a primary peak with a smaller secondary peak or shoulder slightly more positive.[30,66] Thus, as observed for 10^{-3} M As(III) solutions, the different peaks can be correlated with the peaks in the single crystal electrodes. Regarding the possibility of using the stripping signals for the chemical determination of As(III) in solution, it is clear that the best surface is the Au(111) electrode because a single sharp peak is obtained, which can provide an amperometric signal higher than that of the rest of the surfaces with minimal peak overlap from interference species.

Au(UTF) Comparison to Single Crystals. Linear stripping voltammetry was used to compare the electrochemical detection of As(III) for the Au(111), Au(Poly), and Au(UTF) electrode surfaces. Figure 5 presents the LSV of the

https://doi.org/10.1021/acs.jpcc.2c05541
J. Phys. Chem. C XXXX, XXX, XXX−XXX

Table 1. Summary of the Main Characteristics of the Stripping Peaks Obtained after the Deposition of As on the Different Gold Electrodes in in 0.1 M $HClO_4$ + 10^{-5} M As(III)

electrode	deposition potential (V)	stripping peak potential (V)	stripping peak charge (μC cm^{-2})	total stripping charge (μC cm^{-2})
Au(111)	0.175	0.280	248 ± 3	248 ± 3
	0.010	0.300	487 ± 6	487 ± 6
Au(110)	0.160	0.270	149 ± 2	443 ± 3
		0.360	294 ± 3	
	0.060	0.270	278 ± 3	572 ± 6
		0.360	294 ± 3	
Au(100)	0.125	0.275	–	443 ± 2.6
		0.350	–	
		0.450	100 ± 1	
	0.010	0.275	–	572 ± 6
		0.350	–	
		0.450	100 ± 1	
Au(poly)	0.170,	0.280	–	382 ± 2
		0.360	–	
		0.460	176 ± 1	
	0.125	0.280	–	397 ± 2
		0.360	–	
		0.460	176 ± 1	
	0.02	0.280	–	447 ± 2
		0.360	–	
		0.460	176 ± 1	

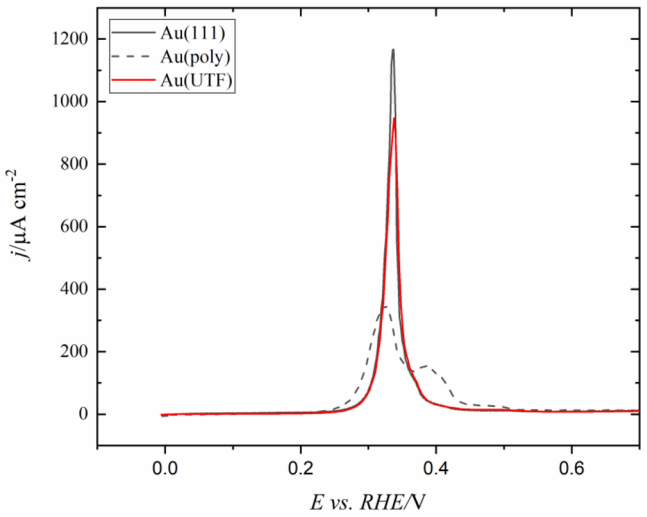

Figure 5. Arsenic stripping voltammograms for the different electrodes in 0.5 M H_2SO_4 + 10^{-5} M As(III). The electrode potential was held for 5 min at 0 V vs RHE. The scan rate is 50 mV s^{-1}.

Au(111) and Au(Poly) single crystals compared to the Au(UTF). The Au(UTF) performed similarly to the Au(111) in 10^{-5} M As(III) solution + 0.5 M H_2SO_4. Table 2 presents a comparison of the maximum peak current potential, full width half-maximum (fwhm), and charge density. The peak potential for the Au(111) and Au(UTF) are 0.337 and 0.338 V, respectively, showing that the binding energy for the stripping process was by and large the same. The maximum peak potential for the Au(poly) electrode was a slightly lower energy at 0.324 V. This may be associated with increased underpotential deposition activity for deposition at Au geometries besides Au(111) which are included in the

Table 2. Summary of the Main Characteristics of the Stripping Peaks Obtained after the Deposition of As on the Different Au Electrodes in 0.5 M H_2SO_4 + 10^{-5} M As(III)

electrode	stripping peak potential (V vs RHE)	full width half max (V vs RHE)	total stripping charge density (μC cm^{-2})
Au(111)	0.337	0.0155	589
Au(poly)	0.324	0.0480	541
Au(UTF)	0.338	0.0206	570

Au(Poly) electrode. The fwhm was determined to identify the capacity for selectivity when other redox active metals may be present in the water matrix. The Au(UTF) and Au(111) surfaces showed fwhm below 20 mV while the Au(Poly) electrode was 48 mV wide which shows that the Au(111) and Au(UTF) have a narrower potential window for detection which may lead to higher selectivity when other metals or electrochemically active species are also present in the water matrix. The peak potential intensity and width of the Au(UTF) electrode is very similar to that of the Au(111) surface, which implies that both surfaces are almost equivalent for this reaction, and that the defects present in the Au(UTF) do not significantly alter the response for this reaction, which is mainly dominated by the presence of (111) grain boundary domains in the Au(UTF).

Au(UTF) Thin Film Calibration Curve. The standard additions method was used to detect trace As(III) in 0.5 M H_2SO_4, and the linear range was determined to be between 2.5 and 50 μg L^{-1}, showing the capability to detect at and below the MCL of 10 μg L^{-1}. For reference, the statistical limit of detection was 0.0065 μg L^{-1}. The blue curve in Figure 6A is the baseline in 0.5 M sulfuric acid. There is a peak near 0.55 V in the baseline that has been observed on other Au(111) surfaces,[54] which disappears upon addition of As(III) even in small concentrations. At concentrations between 2.5 and 17.5 μg L^{-1}, the peak is quite broad beginning near 0.25 V and ends near 0.6 V (Figure 6A). However, at 50 μg L^{-1}, the current increases sharply at 0.25, presenting a peak at 0.35 with a shoulder that ends near 0.6 V. The 100 μg L^{-1} LSV follows a similar peak shape as the 50 μg L^{-1} concentration, however with a larger increase in the peak area at 0.35 V than in the broad region that the lower concentration analysis had. This peak shape change with concentration impacted the linearity when plotting the peak area vs the concentration and resulted in an adjusted R^2 of 0.983 between 2.5 and 50 μg L^{-1} (Figure 6B). Additionally, the R^2 value is increased to 0.998 between 2.5 and 17.5 μg L^{-1} As(III) (Figure S6), showing higher linearity within ±7.5 μg L^{-1} of the 10 μg L^{-1} MCL. Zhang et. al[33] have shown R^2 values of 0.991 and 0.990 with bulk Au and 5 nm Au nanoparticle electrodes between 0.75 and 7.5 μg L^{-1}. As shown in the voltammetric profiles of the single crystal electrodes, the region above 0.3 V should be related to the stripping of the As UPD. Because the Au(111) electrode does not show any characteristic peak in this region, the signal appearing for low concentrations should be related to the presence of defects on the surface, mainly composed of (110) and (100) steps. Those sites are generally more reactive, and thus they are occupied in the early stages of the deposition, giving rise to the formation of a wide wave.

The Au(UTF) electrode addresses availability and usability of aqueous As detection while incorporating enhanced sensitivity and selectivity from controlled surface morphology. This study also considers practicality by using a readily

https://doi.org/10.1021/acs.jpcc.2c05541
J. Phys. Chem. C XXXX, XXX, XXX−XXX

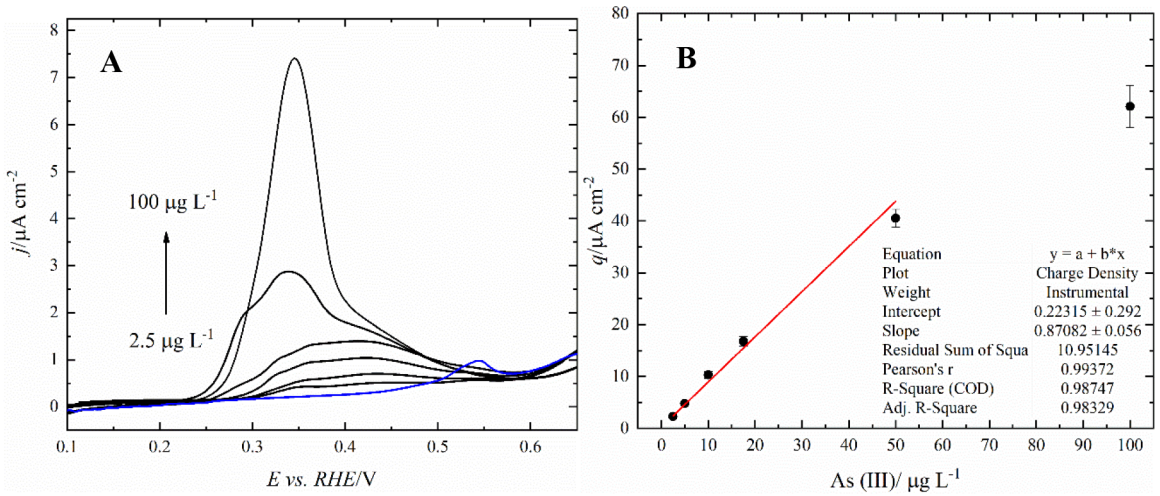

Figure 6. (A) Linear stripping voltammetry analysis curves of baseline 0.5 M H_2SO_4 and standard additions between 2.5 and 100 $\mu g\ L^{-1}$ of As(III) solution. (B) Calibration curve of charge density calculated from the area under the curve and a linear regression curve for data between 2.5 and 50 $\mu g\ L^{-1}$.

available thin film material that does not have to be prepared in situ by Au electrodeposition. In considering a system which can be used by someone without an electrochemical analysis background it is important that the system use methods which do not require electroanalytical optimization and is easily automated. Therefore, we place extra emphasis on the ability to use linear stripping voltammetry instead of more complicated pulse stripping methods while achieving similar or better selectivity in the form of small As(III) oxidation peak widths.[82] This study also utilizes a thin and ultraflat film of Au (~100 nm) which greatly reduces the amount of Au consumed per electrode in comparison to other available single crystals or even unoriented screen printed electrodes.

CONCLUSIONS

This study provides a single crystal model analysis of As deposition and stripping at the basal plane surfaces to provide concise and isolated observations of the effects of surface structure on electrochemical As(III) detection at Au surfaces. This systematic study enabled us to observe that ultraflat Au(111)-oriented thin film electrodes duplicate or exceed the behavior of (111) gold crystal surfaces for As electroanalyses. Stripping of As from the basal plane surfaces showed that the Au(111) model electrode had the highest sensitivity and selectivity as evidenced by having the highest maximum peak current and thinnest oxidation peak compared to the other surfaces. Electrochemical QCM data showed that the deposition of As(III) onto the Au surface occurs in multiple layers, and for each As atom adsorbed, approximately two water molecules are displaced from the surface. The QCM also showed that the stripping of the layers returns the surface to the original state without restructuring or irreversible adsorption of As onto the Au surface. Ultraflat Au(111) thin films performed highly similar to the Au(111) model electrode for As(III) stripping during LSV analysis. Finally, the Au(UTF) was used to detect linearly between 2.5 and 50 $\mu g\ L^{-1}$ As(III) in ultrapure water with 0.5 M H_2SO_4 supporting electrolyte with a theoretical limit of detection of 0.0065 $\mu g\ L^{-1}$. Note that single crystal-like detection capabilities are achievable with minimal (~2 μg) quantities of Au on glass substrates, thus identifying an economically viable and high sensitivity and selectivity electrode. The use of Au (111) texture thin film electrodes with subnanometer roughness may impact many other areas of electroanalysis, as Au electrodes are very commonly used for a large variety of electrochemical investigations.

ASSOCIATED CONTENT

Supporting Information

The Supporting Information is available free of charge at https://pubs.acs.org/doi/10.1021/acs.jpcc.2c05541.

Physical and electrochemical characterization of the system and electrodes, as well as a comparison of linear regression analysis of the calibration curves (PDF)

AUTHOR INFORMATION

Corresponding Authors

Fernando H. Garzon − *Center for Micro-Engineered Materials, University of New Mexico, Albuquerque, New Mexico 87106, United States;* orcid.org/0000-0002-4511-9932; Email: garzon@unm.edu

Tybur Q. Casuse-Driovínto − *Department of Civil, Construction & Environmental Engineering, 1 University of New Mexico, Albuquerque, New Mexico 87131, United States; Center for Micro-Engineered Materials, University of New Mexico, Albuquerque, New Mexico 87106, United States;* orcid.org/0000-0003-0685-0084; Phone: (001) 505-934-6971; Email: tcasuse@unm.edu; Fax: (001) 505-277-1988

Authors

Rubén Rizo − *Instituto de Electroquímica, Universidad de Alicante, E'0308 Alicante, Spain;* orcid.org/0000-0001-8161-2989

Angelica Benavidez − *Center for Micro-Engineered Materials, University of New Mexico, Albuquerque, New Mexico 87106, United States*

Adrian J. Brearley − *Center for Micro-Engineered Materials, University of New Mexico, Albuquerque, New Mexico 87106, United States; Department of Earth & Planetary Sciences, MSC03 2040, 1 University of New Mexico, Albuquerque, New Mexico 87131, United States*

https://doi.org/10.1021/acs.jpcc.2c05541
J. Phys. Chem. C XXXX, XXX, XXX−XXX

José M. Cerrato − *Department of Civil, Construction & Environmental Engineering, 1 University of New Mexico, Albuquerque, New Mexico 87131, United States; Center for Micro-Engineered Materials, University of New Mexico, Albuquerque, New Mexico 87106, United States;* orcid.org/0000-0002-2473-6376

Enrique Herrero − *Instituto de Electroquímica, Universidad de Alicante, E'0308 Alicante, Spain;* orcid.org/0000-0002-4509-9716

Juan M. Feliu − *Instituto de Electroquímica, Universidad de Alicante, E'0308 Alicante, Spain;* orcid.org/0000-0003-4751-3279

Complete contact information is available at: https://pubs.acs.org/10.1021/acs.jpcc.2c05541

Notes

The authors declare no competing financial interest.

■ ACKNOWLEDGMENTS

This material is based upon work supported by the National Science Foundation (NSF) Graduate Research Fellowship Program (GRFP) under grant no. (DGE-1418062), University of New Mexico Center for Water and the Environment, (NSF CREST grant no. 1345169 and 1914490) and the Center for Micro-Engineered Materials (NSF MRI Award DMR-1828731). We thank NanoEarth's Multicultural and Underserved Nanoscience Initiative and the Nanoscale Characterization and Fabrication Laboratory at Virginia Tech (NSF ECCS 1542100 and ECCS 2025151) along with Ya Peng Yu for their aid in providing the EBSD and pole figure data for the Au(UTF) thin films. Scanning transmission electron microscopy was performed in the Nanomaterials Characterization Facility at the University of New Mexico. Thanks to the Fulbright U.S. Scholar Senior Research Award to Spain for Professor Cerrato to collaborate with the Universidad de Alicante. The authors also thank all our colleagues at the Universidad de Alicante for their guidance, generosity, and friendship. Any opinion, findings, and conclusions or recommendations expressed in this material are those of the authors(s) and do not necessarily reflect the views of the National Science Foundation.

■ REFERENCES

(1) Podgorski, J.; Berg, M. Global threat of arsenic in groundwater. *Science* **2020**, *368* (6493), 845−850.

(2) Blake, J. M.; Avasarala, S.; Artyushkova, K.; Ali, A.-M. S.; Brearley, A. J.; Shuey, C.; Robinson, W. P.; Nez, C.; Bill, S.; Lewis, J.; et al. Elevated Concentrations of U and Co-occurring Metals in Abandoned Mine Wastes in a Northeastern Arizona Native American Community. *Environ. Sci. Technol.* **2015**, *49* (14), 8506−8514.

(3) Sikdar, S.; Kundu, M. A Review on Detection and Abatement of Heavy Metals. *ChemBioEng. Rev.* **2018**, *5* (1), 18−29.

(4) WHO. *Arsenic Fact Sheet*. World Health Organization, 2010. https://www.who.int/news-room/fact-sheets/detail/arsenic (accessed 07/21/2022).

(5) USEPA. *Priority Pollutant List*, 2014; Vol. *40*, CFR Part 423, Appendix A.

(6) Ferguson, J. F.; Gavis, J. Review of the arsenic cycle in natural waters. *Water Res.* **1972**, *6*, 1259−1274 Article.

(7) Korte, N. E. Q.; Fernando, Q. Fernando. A review of arsenic(III) in groundwater. *Crit. Rev. Environ. control* **1991**, *21*, 1−39.

(8) Forsberg, G.; Olaughlin, J. W.; Megargle, R. G.; Koirtyohann, S. R. Determination of arsenic by anodic stripping voltammetry and differential pulse anodic stripping voltammetry. *Anal. Chem.* **1975**, *47*, 1586−1592.

(9) Smedley, P. L.; Kinniburgh, D. G. A review of the source, behaviour and distribution of arsenic in natural waters. *Appl. Geochem.* **2002**, *17*, 517−568.

(10) Stuckey, J. W.; Schaefer, M. V.; Kocar, B. D.; Benner, S. G.; Fendorf, S. Arsenic release metabolically limited to permanently water-saturated soil in Mekong Delta. *Nat. Geosci.* **2016**, *9* (1), 70−76.

(11) LeMonte, J. J.; Stuckey, J. W.; Sanchez, J. Z.; Tappero, R.; Rinklebe, J.; Sparks, D. L. Sea Level Rise Induced Arsenic Release from Historically Contaminated Coastal Soils. *Environ. Sci. Technol.* **2017**, *51* (11), 5913−5922.

(12) deLemos, J. L.; Bostick, B. C.; Renshaw, C. E.; StÜrup, S.; Feng, X. Landfill-Stimulated Iron Reduction and Arsenic Release at the Coakley Superfund Site (NH). *Environ. Sci. Technol.* **2006**, *40* (1), 67−73.

(13) He, C.; Tao, M.; Zhang, C.; He, Y.; Xu, W.; Liu, Y.; Zhu, W. Microelectrode-Based Electrochemical Sensing Technology for in Vivo Detection of Dopamine: Recent Developments and Future Prospects. *Crit. Rev. Environ. Control* **2022**, *52*, 544−554.

(14) Dai, X.; Wildgoose, G. G.; Salter, C.; Crossley, A.; Compton, R. G. Electroanalysis using macro-, micro-, and nanochemical architectures on electrode surfaces. Bulk surface modification of glassy carbon microspheres with gold nanoparticles and their electrical wiring using carbon nanotubes. *Anal. Chem.* **2006**, *78* (17), 6102−6108.

(15) Fleischmann, M.; Pons, S. The behavior of microelectrodes. *Anal. Chem.* **1987**, *59* (24), 1391A−1399A.

(16) Compton, R. G.; Wildgoose, G. G.; Rees, N. V.; Streeter, I.; Baron, R. Design, fabrication, characterisation and application of nanoelectrode arrays. *Chem. Phys. Lett.* **2008**, *459* (1), 1−17.

(17) Das, J.; Sarkar, P.; Panda, J.; Pal, P. Low-cost field test kits for arsenic detection in water. *J. Environ. Sci. Health., A* **2014**, *49* (1), 108−115.

(18) Bullen, J. C.; Torres-Huerta, A.; Salaun, P.; Watson, J. S.; Majumdar, S.; Vilar, R.; Weiss, D. J. Portable and rapid arsenic speciation in synthetic and natural waters by an As(V)-selective chemisorbent, validated against anodic stripping voltammetry. *Water Res.* **2020**, *175*, 115650.

(19) Nunez-Bajo, E.; Blanco-Lopez, M. C.; Costa-Garcia, A.; Fernandez-Abedul, M. T. Electrogeneration of Gold Nanoparticles on Porous-Carbon Paper-Based Electrodes and Application to Inorganic Arsenic Analysis in White Wines by Chronoamperometric Stripping. *Anal. Chem.* **2017**, *89* (12), 6415−6423.

(20) Thangphatthanarungruang, J.; Lomae, A.; Chailapakul, O.; Chaiyo, S.; Siangproh, W. A Low-cost Paper-based Diamond Electrode for Trace Copper Analysis at On-site Environmental Area. *Electroanalysis* **2021**, *33* (1), 226−232.

(21) Borrill, A. J.; Reily, N. E.; Macpherson, J. V. Addressing the practicalities of anodic stripping voltammetry for heavy metal detection: a tutorial review. *Analyst* **2019**, *144* (23), 6834−6849.

(22) Cox, J. A.; Rutkowska, I. A.; Kulesza, P. J. Critical Review—Electrocatalytic Sensors for Arsenic Oxo Species. *J. Electrochem. Soc.* **2020**, *167* (3), 037565.

(23) Buffa, A.; Mandler, D. Arsenic(III) detection in water by flow-through carbon nanotube membrane decorated by gold nanoparticles. *Electrochim. Acta* **2019**, *318*, 496−503.

(24) Dai, X.; Nekrassova, O.; Hyde, M. E.; Compton, R. G. Anodic Stripping Voltammetry of Arsenic(III) Using Gold Nanoparticle-Modified Electrodes. *Anal. Chem.* **2004**, *76*, 5924−5929.

(25) Devi, N. R.; Sasidharan, M.; Sundramoorthy, A. K. Gold Nanoparticles-Thiol-Functionalized Reduced Graphene Oxide Coated Electrochemical Sensor System for Selective Detection of Mercury Ion. *J. Electrochem. Soc.* **2018**, *165* (8), B3046−B3053.

(26) Garcia-Gonzalez, R.; Fernandez-Abedul, M. T.; Costa-Garcia, A. Nafion(R) modified-screen printed gold electrodes and their carbon nanostructuration for electrochemical sensors applications. *Talanta* **2013**, *107*, 376−381.

(27) Gu, T.; Bu, L.; Huang, Z.; Liu, Y.; Tang, Z.; Liu, Y.; Huang, S.; Xie, Q.; Yao, S.; Tu, X.; et al. Dual-signal anodic stripping voltammetric determination of trace arsenic(III) at a glassy carbon electrode modified with internal-electrolysis deposited gold nanoparticles. *Electrochem. Commun.* **2013**, *33*, 43−46.
(28) Hamilton, T. W.; Florence, T. M.; Ellis, J. Determination of arsenic and antimony in electrolytic copper by anodic stripping voltammetry at a gold film electrode. *Anal. Chim. Acta* **1980**, *119* (2), 225−233.
(29) Huang, J.-F.; Chen, H.-H. Gold-nanoparticle-embedded nafion composite modified on glassy carbon electrode for highly selective detection of arsenic(III). *Talanta* **2013**, *116*, 852−859.
(30) Casuse, T. Q.; Benavidez, A.; Plumley, J. B.; Tsui, L.-k.; Ali, A.-M.; Cerrato, J. M.; Garzon, F. H. DC Sputtered Ultralow Loading Gold Nanofilm Electrodes for Detection of As(III) in Water. *ECS Sens. Plus* **2022**, *1* (1), 014602.
(31) Udayan, A. P. M.; Kachwala, B.; Karthikeyan, K. G.; Gunasekaran, S. Ultrathin quasi-hexagonal gold nanostructures for sensing arsenic in tap water. *RSC Adv.* **2020**, *10* (34), 20211−20221.
(32) Jia, Z.; Simm, A. O.; Dai, X.; Compton, R. G. The electrochemical reaction mechanism of arsenic deposition on an Au(111) electrode. *J. Electroanal. Chem.* **2006**, *587* (2), 247−253.
(33) Zhang, Y.; Li, D.; Compton, R. G.Arsenic(III) detection with underpotential deposition on gold. *J. Electroanal. Chem.***2022**, *909*. 116154.
(34) Kastro, K. C.Effect of Nanostructures of Au Electrodes on the Electrochemical Detection of As.*J. Electrochem. Sci. Technol.***2019**, *10*.
(35) Salinas, S.; Mosquera, N.; Luis, Y.; Emerson, C.; Germán, Y.; Edgar, G. Surface Plasmon Resonance Nanosensor for the Detection of Arsenic in Water. *Sens. Transducers* **2014**, *183* (12), 97−102.
(36) Zhang, Y.; Li, D.; Compton, R. G. Arsenic(III) Detection with Underpotential Deposition and Anodic Stripping Voltammetry. *ChemElectroChem.* **2021**, *8* (19), 3707−3715.
(37) Kopanica, M.; Novotný, L. Determination of traces of arsenic(III) by anodic stripping voltammetry in solutions, natural waters and biological material. *Anal. Chim. Acta* **1998**, *368* (3), 211−218.
(38) Xiao, L.; Wildgoose, G. G.; Compton, R. G. Sensitive electrochemical detection of arsenic(III) using gold nanoparticle modified carbon nanotubes via anodic stripping voltammetry. *Anal. Chim. Acta* **2008**, *620* (1), 44−49.
(39) Rahman, M. R.; et al. Selective Detection of As(III) at the Au(111)-like Polycrystalline Gold Electrode. *Anal. Chem.* **2010**, *82* (22), 9169−9176.
(40) El-Deab, M. S.; Arihara, K.; Ohsaka, T. Fabrication of Au(111)-Like Polycrystalline Gold Electrodes and Their Applications to Oxygen Reduction. *J. Electrochem. Soc.* **2004**, *151* (6), No. E213.
(41) Ren, B.; Jones, L. A.; Chen, M.; Oppedisano, D. K.; Qiu, D.; Ippolito, S. J.; Bhargava, S. K. The Effect of Electrodeposition Parameters and Morphology on the Performance of Au Nanostructures for the Detection of As(III). *J. Electrochem. Soc.* **2017**, *164* (14), H1121−H1128.
(42) Han, D.-D.; Li, S.-S.; Guo, Z.; Chen, X.; Liu, J.-H.; Huang, X.-J. Shape dependent stripping behavior of Au nanoparticles toward arsenic detection: evidence of enhanced sensitivity on the Au (111) facet. *RSC Adv.* **2016**, *6* (36), 30337−30344.
(43) Jiang, X.; Ma, J.; Jiang, G.; Xu, M.; Huang, X.; Gao, G.; Dai, X. Preparation of Gold Nanoplates Using Ortho Carbonyl Compounds as Capping Agents for Electrochemical Sensing of Lead Ions. *Nanoscale Res. Lett.* **2021**, *16* (1), 57.
(44) Babar, N. U.; Joya, K. S.; Tayyab, M. A.; Ashiq, M. N.; Sohail, M. Highly Sensitive and Selective Detection of Arsenic Using Electrogenerated Nanotextured Gold Assemblage. *ACS Omega* **2019**, *4* (9), 13645−13657.
(45) Snyder, J.; Danilovic, N.; Paulikas, A. P.; Tripkovic, D.; Strmcnik, D.; Markovic, N. M.; Stamenkovic, V. R. Thin Film Approach to Single Crystalline Electrochemistry. *J. Phys. Chem. C* **2013**, *117* (45), 23790−23796.
(46) Kishioka, S.-y.; Nishino, J.; Sakaguchi, H. Fabrication of Stable, Highly Flat Gold Film Electrodes with an Effective Thickness on the Order of 10 nm. *Anal. Chem.* **2007**, *79* (17), 6851−6856.
(47) Technologies, P.*Ultra-Flat Gold Surfaces*. https://www.platypustech.com/gold-thin-films/ultra-flat-gold-films (accessed 10/25/2021).
(48) Duan, H.et al.High-Performance Rh2P Electrocatalyst for Efficient Water Splitting. *J. Am. Chem. Soc.***2017***139* (15), 5494−5502. From http://worldcat.org/z-wcorg/.
(49) Wei, C.; Rao, R. R.; Peng, J. Y.; Huang, B. T.; Stephens, I. E. L.; Risch, M.; Xu, Z. C. J.; Shao-Horn, Y.Recommended Practices and Benchmark Activity for Hydrogen and Oxygen Electrocatalysis in Water Splitting and Fuel Cells. *Adv. Mater.***2019**, *31* (31). 1806296.
(50) Sajfutdinow, M.; Uhlig, K.; Prager, A.; Schneider, C.; Abel, B.; Smith, D. M. Nanoscale patterning of self-assembled monolayer (SAM)-functionalised substrates with single molecule contact printing. *Nanoscale* **2017**, *9* (39), 15098−15106.
(51) Kuzume, A.; Herrero, E.; Feliu, J. M. Oxygen reduction on stepped platinum surfaces in acidic media. *J. Electroanal. Chem.* **2007**, *599* (2), 333−343.
(52) Feliu, J. M.; Fernandez-Vega, A.; Aldaz, A.; Clavilier, J. New observations of a structure sensitive electrochemical behaviour of irreversibly adsorbed arsenic and antimony from acidic solutions on Pt (111) and Pt (100) orientations. *J. Electroanal. Chem. Interfacial Electrochem.* **1988**, *256* (1), 149−163.
(53) Rizo, R.; Pastor, E.; Koper, M. T. M. CO electrooxidation on Sn-modified Pt single crystals in acid media. *J. Electroanal. Chem.* **2017**, *800*, 32−38 Article.
(54) Fang, Y.; Ding, S. Y.; Zhang, M.; Steinmann, S. N.; Hu, R.; Mao, B. W.; Feliu, J. M.; Tian, Z. Q. Revisiting the Atomistic Structures at the Interface of Au(111) Electrode-Sulfuric Acid Solution. *J. Am. Chem. Soc.* **2020**, *142* (20), 9439−9446.
(55) Gisbert-González, J. M.; Oliver-Pardo, M. V.; Sarabia, F. J.; Climent, V.; Feliu, J. M.; Herrero, E.On the behavior of CTAB/CTAOH adlayers on gold single crystal surfaces. *Electrochim. Acta***2021**, *391*. 138947.
(56) Rodes, A.; Herrero, E.; Feliu, J. M.; Aldaz, A. Structure sensitivity of irreversibly adsorbed tin on gold single-crystal electrodes in acid media. *J. Chem. Soc. Faraday Trans.* **1996**, *92* (20), 3769−3776.
(57) Hamelin, A. Underpotential deposition of lead on single crystal faces of gold: Part I. The influence of crystallographic orientation of the substrate. *J. Electroanal. Chem. Interfacial Electrochem.* **1984**, *165* (1), 167−180.
(58) Hamelin, A.; Lipkowski, J. Underpotential deposition of lead on gold single crystal faces: Part II. General discussion. *J. Electroanal. Chem. Interfacial Electrochem.* **1984**, *171* (1), 317−330.
(59) Lebedeva, N. P.; Rodes, A.; Feliu, J. M.; Koper, M. T. M.; van Santen, R. A. Role of Crystalline Defects in Electrocatalysis: CO Adsorption and Oxidation on Stepped Platinum Electrodes As Studied by in situ Infrared Spectroscopy. *J. Phys. Chem. B* **2002**, *106* (38), 9863−9872.
(60) Bentley, C. L.; Kang, M.; Unwin, P. R. Nanoscale Surface Structure-Activity in Electrochemistry and Electrocatalysis. *J. Am. Chem. Soc.* **2019**, *141* (6), 2179−2193.
(61) van der Zalm, J.; Chen, S.; Huang, W.; Chen, A. Review—Recent Advances in the Development of Nanoporous Au for Sensing Applications. *J. Electrochem. Soc.* **2020**, *167* (3), 037532.
(62) Liu, Z.-G.; Huang, X.-J. Voltammetric determination of inorganic arsenic. *TrAC Trends in Analytical Chemistry* **2014**, *60*, 25−35.
(63) Guo, Z.; Yang, M.; Huang, X.-J. Recent developments in electrochemical determination of arsenic. *Current Opinion in Electrochemistry* **2017**, *3* (1), 130−136 Review Article.
(64) Mardegan, A.; Scopece, P.; Lamberti, F.; Meneghetti, M.; Moretto, L. M.; Ugo, P. Electroanalysis of Trace Inorganic Arsenic with Gold Nanoelectrode Ensembles. *Electroanalysis* **2012**, *24* (4), 798−806.

https://doi.org/10.1021/acs.jpcc.2c05541
J. Phys. Chem. C XXXX, XXX, XXX−XXX

(65) Basu, A.; Saha, D.; Saha, R.; Ghosh, T.; Saha, B. A review on sources, toxicity and remediation technologies for removing arsenic from drinking water. *Res. Chem. Intermed.* **2014**, *40* (2), 447−485 Article.
(66) Jena Bikash Kumar, B. K.; Raj, C. R. Gold nanoelectrode ensembles for the simultaneous electrochemical detection of ultratrace arsenic, mercury, and copper. *Anal. Chem.* **2008**, *80* (13), 4836−4844.
(67) Berg, M. M.; et al. Arsenic contamination of groundwater and drinking water in Vietnam: a human health threat. *Environ. Sci. Technol.* **2001**, *35* (13), 2621−2626.
(68) Hu, H. B.; Xie, B.; Lu, Y.; Zhu, J. Advances in Electrochemical Detection Electrodes for As(III). *Nanomaterials* **2022**, *12* (5), 781.
(69) Liu, Y.; Xue, Q.; Chang, C.; Wang, R.; Liu, Z.; He, L.Recent Progress regarding Electrochemical Sensors for the Detection of Typical Pollutants in Water Environments. *Anal. Sci.***2022**, *38*. 55.
(70) Clavilier, J.; Faure, R.; Guinet, G.; Durand, R. Preparation of monocrystalline Pt microelectrodes and electrochemical study of the plane surfaces cut in the direction of the {111} and {110} planes. *J. Electroanal. Chem. Interfacial Electrochem.* **1980**, *107* (1), 205−209.
(71) Hamelin, A. Cyclic voltammetry at gold single-crystal surfaces. Part 1. Behaviour at low-index faces. *J. Electroanaly. Chem.* **1996**, *407*, 1−11.
(72) Dinan, T. E.; Jou, W. F.; Cheh, H. Y. Arsenic Deposition onto a Gold Substrate. *J. Electrochem. Soc.* **1989**, *136* (11), 3284−3287.
(73) Enting, I. G. Crystal growth models and Ising models. II. Constraints on high-field expansions. *J. Phys. A: Math. Gen.* **1977**, *10* (6), 1023−1030.
(74) Scherb, G.; Kazimirov, A.; Zegenhagen, J.; Schultz, T.; Feidenhans'l, R.; Fimland, B. O. Potential controlled stripping of an amorphous As layer on GaAs(001) in an electrolyte: An in situ x-ray scattering study. *Appl. Phys. Lett.: United States* **1997**, *71*, 2990−2992.
(75) Kolb, D. M. Electrochemical Surface Science. *Angew. Chem., Int. Ed.* **2001**, *40* (7), 1162−1181 (acccessed 2022/06/03).
(76) Blum, L.; Huckaby, D. A. Underpotential deposition of Cu on Au(111): implications of the HB model. *J. Electroanal. Chem.* **1994**, *375* (1), 69−77.
(77) Orozco, J.; Fernández-Sánchez, C.; Jiménez-Jorquera, C. Underpotential Deposition-Anodic Stripping Voltammetric Detection of Copper at Gold Nanoparticle-Modified Ultramicroelectrode Arrays. *Environ. Sci. Technol.* **2008**, *42* (13), 4877−4882.
(78) Desimoni, E.; Palmisano, F.; Sabbatini, L. Simultaneous determination of tin and lead at the parts-per-billion level by coupling differential pulse anodic stripping voltammetry with a matrix exchange method. *Anal. Chem.* **1980**, *52* (12), 1889−1892.
(79) Villegas, I.; Stickney, J. L. Preliminary Studies of GAAS Deposition on Au(100), (110), and (111) Surfaces by Electrochemical Atomic Layer Epitaxy. *J. Electrochem. Soc.* **1992**, *139* (3), 686−694.
(80) Huang, S.-Q.; Huang, Z.; Gu, T.-A.; Xie, Q.-J.; Yao, S.-Z. Study of Electrochemical Behaviour of As(III) at Au/Au and Pt/Au Electrodes by Electrochemical Quartz Crystal Microbalance. *Chin. J. Anal. Chem.* **2011**, *39* (7), 978−984.
(81) Innocenti, M.; Forni, F.; Pezzatini, G.; Raiteri, R.; Loglio, F.; Foresti, M. L. Electrochemical behavior of As on silver single crystals and experimental conditions for InAs growth by ECALE. *J. Electroanal. Chem.* **2001**, *514* (1), 75−82.
(82) Bard, A. J.; Faulkner, L. R.Polarography and Pulse Voltammetry. In *Electrochemical Methods: Fundamentals and Applications*; John Wiley & Sons, 2001; Chapter 7, pp 275−301.

https://doi.org/10.1021/acs.jpcc.2c05541
J. Phys. Chem. C XXXX, XXX, XXX−XXX